LJMU Research Online

Anguiano, B, Mitschang, AW, Kirihara, T, Hirai, Y, Horta, D, Hasselquist, S, Piorno Schiavon, R, Majewski, SR, Mason, AC, Price-Whelan, AM, Prieto, CA, Smith, VV, Cunha, K and Nidever, DL

 Tidal Debris Candidates from the ω Centauri Accretion Event and Its Role Building Up the Milky Way Halo

https://researchonline.ljmu.ac.uk/id/eprint/26889/

Article

Tidal Debris Candidates from the ω Centauri Accretion Event and Its Role Building Up the Milky Way Halo

Borja Anguiano[1,2,15] , Arik W. Mitschang[3] , Takanobu Kirihara[4] , Yutaka Hirai[5] , Danny Horta[6] , Sten Hasselquist[7] , Ricardo P. Schiavon[8] , Steven R. Majewski[2] , Andrew C. Mason[8] , Adrian M. Price-Whelan[6] , Carlos Allende Prieto[9,10] , Verne V. Smith[11] , Katia Cunha[12,13] , and David L. Nidever[14]

[1] Centro de Estudios de Física del Cosmos de Aragón (CEFCA), Plaza San Juan 1, 44001, Teruel, Spain; banguiano@cefca.es
[2] Department of Astronomy, University of Virginia, Charlottesville, VA 22904-4325, USA
[3] Henry A. Rowland Department of Physics and Astronomy, The Johns Hopkins University, Baltimore, MD 21218, USA
[4] Kitami Institute of Technology, 165, Koen-cho, Kitami, Hokkaido 090-8507, Japan
[5] Department of Community Service and Science, Tohoku University of Community Service and Science, 3-5-1 Iimoriyama, Sakata, Yamagata 998-8580, Japan
[6] University of Edinburgh, Royal Observatory, Blackford Hill, Edinburgh, EH9 3HJ, UK
[7] Space Telescope Science Institute, 3700 San Martin Drive, Baltimore, MD 21218, USA
[8] Astrophysics Research Institute, Liverpool John Moores University, 146 Brownlow Hill, Liverpool L3 5RF, UK
[9] Instituto de Astrofísica de Canarias, E-38205 La Laguna, Tenerife, Spain
[10] Universidad de La Laguna, Dpto. Astrofísica, E-38206 La Laguna, Tenerife, Spain
[11] National Optical Astronomy Observatories, Tucson, AZ 85719, USA
[12] Steward Observatory, University of Arizona, 933 North Cherry Avenue, Tucson, AZ 85721-0065, USA
[13] Observatório Nacional/MCTIC, R. Gen. José Cristino, 77, 20921-400, Rio de Janeiro, Brazil
[14] Department of Physics, Montana State University, PO Box 173840, Bozeman, MT 59717-3840, USA

Abstract

We identify stellar tidal debris from the ω Centauri (ω Cen) system among field stars in the Apache Point Observatory Galactic Evolution Experiment (APOGEE) survey via chemical tagging using a neural network trained on APOGEE observations of the ω Cen core. We find a total of 463 ω Cen debris candidates have a probability $P > 0.8$ of sharing common patterns in their chemical abundances across a range of individual elements or element combinations, including [C+N], O, Mg, Al, Si, Ca, Ni, and Fe. Some debris candidates show prograde or retrograde disk-like kinematics, but most show kinematics consistent with the accreted halo, showing high radial actions, J_R, values. We find that a sample of Gaia-Sausage-Enceladus (GES) members are chemically distinct from the ω Cen core, suggesting that ω Cen is associated with an independent merger event shaping the Milky Way halo. However, a connection between GSE and ω Cen cannot be ruled out. A detailed comparison with N-body simulations indicates that the ω Cen progenitor was a massive dwarf galaxy ($\gtrsim 10^8 M_\odot$). The existence of a metal-poor high-α chemically homogeneous halo debris is also reported.

Unified Astronomy Thesaurus concepts: Globular star clusters (656); Milky Way stellar halo (1060)

Materials only available in the online version of record: machine-readable table

1. Introduction

The "globular cluster" ω Centauri (ω Cen) has a number of peculiar characteristics that set it apart from other Milky Way globular clusters; these include its very large mass, extended size, oblate shape, internal rotation, large age and metallicity spreads (G. Piotto et al. 2005; A. Bellini et al. 2010; C. I. Johnson & C. A. Pilachowski 2010; S. Villanova et al. 2014), and a retrograde orbit only slightly inclined to the Galactic plane (D. I. Dinescu 2002; E. Vasiliev 2019). Because of these properties, together with its peculiar surface brightness profile, it is believed that ω Cen may be the core remnant of a heavily stripped, Milky Way–captured dwarf spheroidal galaxy, now currently orbiting retrograde near the Galactic plane (e.g., Y. W. Lee et al. 1999; S. R. Majewski et al. 2000; K. Bekki & K. C. Freeman 2003; T. Tsuchiya et al. 2003, 2004; M. Ideta & J. Makino 2004). In a few, generally massive

globular clusters where ω Cen represents the most extreme case, different internal stellar populations show abundance variations of virtually all elements, suggesting that these massive clusters might be considered as an intermediate evolutionary stage between globular clusters and ultra compact dwarf galaxies (e.g., D. A. Forbes & P. Kroupa 2011; M. A. Norris & S. J. Kannappan 2011). Additionally, E. Noyola et al. (2008) detected a rise in velocity dispersion from 18.6 km s^{-1} at 14″ to 23 km s^{-1} in the center; a rise associated with the existence of an intermediate-mass black hole. Z. Cheng et al. (2020), using X-ray sources as sensitive probes of stellar dynamical interactions, also reported the existence of a black hole subsystem in ω Cen. Recently, M. Häberle et al. (2024), using fast-moving stars in the central region of the cluster, reported the existence of an intermediate-mass black hole with a mass of ∼8200 $M_\odot$. Moreover, potentially accreted stellar systems have been reported within the cluster (e.g., F. R. Ferraro et al. 2002; A. Calamida et al. 2020). These findings imply that ω Cen has galaxy-like properties.

There is now strong evidence to indicate active tidal disruption of ω Cen, with the detection of tidal tails extending directly from the system finally identified by R. A. Ibata et al. (2019) and

P. B. Kuzma & M. N. Ishigaki (2025), after years of negative, uncertain or low-significance detections for this expected phenomenon (e.g., S. Leon et al. 2000; D. R. Law et al. 2003; G. S. Da Costa & M. G. Coleman 2008; E. Wylie-de Boer et al. 2010; B. Anguiano et al. 2015; J. G. Fernández-Trincado et al. 2015). R. A. Ibata et al. (2019) also reported that the Fimbulthul structure is a tidal stream of ω Cen (see also J. D. Simpson et al. 2020). Furthermore, the main chemical properties of ω Cen can be reproduced if it is the compact remnant of a dwarf spheroidal galaxy that evolved in isolation and then was accreted and partly disrupted by the Milky Way's tidal forces. The ingested satellite would also have chemical properties similar to the core of ω Cen (D. Romano et al. 2007). N-body/gas dynamical simulations of the formation and evolution of ω Cen (G. Carraro & C. Lia 2000; T. Tsuchiya et al. 2004) reproduce the bulk properties of the cluster—namely its structure, kinematics, and chemistry—assuming that this stellar system formed and evolved in isolation, and eventually fell inside the Milky Way potential well. G. Carraro & C. Lia (2000) concluded that ω Cen could actually be a cosmological dwarf by mass, a system formed in a high redshift low mass halo that escaped significant merging up to the present time. Moreover, A. Meza et al. (2005) used numerical simulations to analyze the dynamical properties of tidal debris stripped from a satellite on a highly eccentric orbit, and they found that these satellites may deposit a significant fraction of their stars in the disk components of a galaxy. Furthermore, using compilations of nearby metal-poor stars, A. Meza et al. (2005) reported a stellar group that based on dynamical and chemical coherence, appears to consist of stars that once belonged to the dwarf that brought ω Cen into the Galaxy.

In the context of the connection between globular clusters and dwarf galaxies, it is widely accepted that the globular cluster M54 is associated with the Sagittarius dwarf spheroidal galaxy (Sgr) and that M54 formed and evolved in the environment of a dwarf spheroidal galaxy (e.g., A. Sarajedini & A. C. Layden 1995; S. R. Majewski et al. 2003; L. Monaco et al. 2005; M. Bellazzini et al. 2008; E. Carretta et al. 2010). The M54/Sgr system is often suggested as the paradigm for a putative former ω Cen progenitor, and this has inspired the search for tidal debris shed from said progenitor now lying among Milky Way field stars. For example, D. I. Dinescu (2002) looked for metal-poor stars in the solar neighborhood that shared ω Cen's orbit. More recently, G. C. Myeong et al. (2018), using Gaia DR2 (A. G. A. Brown et al. 2018), discovered a new retrograde substructure in the Milky Way halo (named the "Sequoia" galaxy), that they associated with the ω Cen progenitor. Their analysis shows the efficacy of using kinematics to identify potential ω Cen stars. However, as we shall show in Section 3.2, retrograde behavior alone—and even orbits of a common angular momentum—are not sufficient evidence of a linkage to ω Cen. For this reason, additional characteristics —such as chemistry—are needed to discriminate ω Cen debris. Alternatively, G. C. Myeong et al. (2018) and D. Massari et al. (2019) studied the age–metallicity relation of Milky Way globular clusters associated with the different halo structures and concluded that ω Cen could have been the nuclear star cluster of the more massive Gaia-Sausage-Enceladus (GSE) galaxy.

Previous searches for more extended ω Cen tidal debris within a large, all-sky low-resolution spectroscopic and photometric catalog of giant stars by S. R. Majewski et al. (2012) identified candidate retrograde stars near the Galactic plane having kinematics (derived solely from radial velocities) consistent with being stripped debris from ω Cen, based on

tidal destruction models of the system. To confirm their status as former ω Cen members, high-resolution spectroscopy was undertaken of a dozen of these candidates, and most were found by S. R. Majewski et al. (2012) to exhibit very high relative Ba abundances (as measured by the $\lambda5854$ Å transition)—a peculiar characteristic apparently unique to the ω Cen system, as originally shown by J. E. Norris & G. S. Da Costa (1995) and V. V. Smith et al. (2000). See also Figure 11 in D. Geisler et al. (2007). Thus, these results showed the likelihood of a connection between a set of widely distributed field stars and ω Cen, which could then be used to make some broad inferences about the orbit of the progenitor.

Although generating a relatively small, though broadly outlying group of ω Cen debris stars, the S. R. Majewski et al. (2012) study demonstrated an effective procedure for selecting candidates according to their chemical fingerprint. Such a procedure can be useful for creating a larger census of ω Cen stars across the Milky Way. With the advent of large-scale Milky Way stellar surveys like Gaia and Apache Point Observatory Galactic Evolution Experiment (APOGEE) providing plentiful and accurate chemo-kinematical data for vastly large numbers of stars, a far more comprehensive search for ω Cen debris stars can be mounted following a similar prescription. In this study, we performed such a larger analysis using accurate multielement chemical abundances from the APOGEE (S. R. Majewski et al. 2017) to search for tidal debris candidates from the ω Cen accretion event.

The concept of chemical tagging consists of using detailed chemical abundances of individual stars to tag them to common ancient star-forming aggregates whose stars have similar abundance patterns (e.g., K. Freeman & J. Bland-Hawthorn 2002; A. W. Mitschang et al. 2013, 2014; G. M. De Silva et al. 2015). The feasibility of chemical tagging has been investigated with promising results (e.g., A. C. Quillen et al. 2015; D. W. Hogg et al. 2016; J. Kos et al. 2018; L. Spina et al. 2022). However, R. Garcia-Dias et al. (2019) and L. Casamiquela et al. (2021) showed that different stellar birth sites can have overlapping chemical signatures, suggesting substantial evidence against the feasibility of a strong chemical tagging. Recently, K. Youakim et al. (2023) used the combined GALAH DR3 (S. Buder et al. 2021) and Gaia eDR3 (Gaia Collaboration et al. 2021) data sets to identify candidates stripped off from ω Cen. Using simultaneously the chemical and dynamical parameter space via an unsupervised clustering algorithm (t-SNE; L. van der Maaten & G. E. Hinton 2008), K. Youakim et al. (2023) reported debris candidates extending more than $50°$ away from the cluster. Recently, G. Pagnini et al. (2025) proposed that at least six Milky Way globular clusters share a common origin with ω Cen, further supporting the hypothesis that this system is the remnant of a galaxy.

In a similar vein, from the combination of full 3D kinematics derived from Gaia proper motions and APOGEE radial velocities, accurate multielement chemical abundances from APOGEE, and distances from the StarHorse value-added catalog (A. B. A. Queiroz et al. 2020), we identify a large sample of several hundred stars sharing ω Cen's peculiar chemical characteristics and use them to constrain the present and past orbital properties of the ω Cen progenitor. With our new sample of ω Cen stars thus identified, a more complete and definitive mapping of ω Cen tidal debris can be built and used to shed further light on its complex chemodynamical evolution. In particular, we conjecture about the possible

association of ω Cen with other, previously identified, major accreted structures in the Milky Way halo.

2. APOGEE and Gaia Data Sets

The APOGEE (S. R. Majewski et al. 2017), part of both SDSS-III (D. J. Eisenstein et al. 2011) and SDSS-IV (M. R. Blanton et al. 2017), explored the multielement chemistry and radial velocities of stars across all stellar populations of the Milky Way using high-resolution ($R \sim 22{,}500$) spectra spanning a large fraction of the H-band (1.5–1.7 μm). APOGEE in SDSS-III, initially operating from the Sloan 2.5 m Telescope (J. E. Gunn et al. 2006) at the Apache Point Observatory, expanded observations to include both hemispheres as part of APOGEE-2 in SDSS-IV through the installation of a twin spectrograph (J. C. Wilson et al. 2019) on the du Pont telescope at Las Campanas Observatory. In addition, the new APOGEE-South spectrograph was used to procure observations of almost 2000 red giant branch (RGB) stars in the ω Cen core (including observations of the system during "first light" commissioning of the instrument—e.g., S. Mészáros et al. 2021). These spectra of the ω Cen core provide critical templates for our Galaxy-wide search for stripped ω Cen counterparts.

We make use of the last SDSS-IV public release of data from the APOGEE Stellar Parameters and Chemical Abundances Pipeline (ASPCAP; A. E. García Pérez et al. 2016; J. A. Holtzman et al. 2018) based on MARCS model atmospheres (B. Gustafsson et al. 2008), SYNSPEC (I. Hubeny et al. 2021), and FERRE (C. Allende Prieto et al. 2006). These data were processed and publicly released within SDSS Data Release 17 (DR17; Abdurro'uf et al. 2022)[16] Using the APOGEE line list (M. Shetrone et al. 2015; S. Hasselquist et al. 2016; K. Cunha et al. 2017; V. V. Smith et al. 2021), the DR17 reduction pipelines deliver $v_{\rm los}$, stellar atmospheric parameters, and abundances for 18 individual chemical species (D. L. Nidever et al. 2015; J. A. Holtzman et al. 2015; A. E. García Pérez et al. 2016; H. Jönsson et al. 2020), some of them considering departures from LTE (Y. Osorio et al. 2020).

In this study, we also exploit data from the third data release (DR3) of the Gaia mission (Gaia Collaboration et al. 2023) through the APOGEE StarHorse value-added catalog (A. B. A. Queiroz et al. 2020). We use the Galactocentric frame in Astropy v5.2.1 (Astropy Collaboration et al. 2022), which contains the following parameters: a solar Galactocentric distance of $R_0 = 8.275$ kpc, a solar motion in cylindrical coordinates of $(v_{R,\odot}, v_{\phi,\odot}, v_{z,\odot}) = (8.4, 251.8, 8.4)$ km s^{-1}, and a solar position with respect to the Galactic midplane of $Z_\odot = 20.8$ pc. We use v1.3 of Gala[17] (A. M. Price-Whelan 2017) to compute actions and other orbital information, and for which we adopt Gaia DR3 astrometry, StarHorse distances, and APOGEE DR17 radial velocities. We used Gala's default gravitational potential from J. Bovy (2015), which is matched to the A.-C. Eilers et al. (2019) rotation curve. In this way, we put together a catalog of orbital properties, such as eccentricities, peri/apocenter radii, maximal disk height Z, orbital actions, frequencies, and angles, together with their uncertainties for all stars. The adopted reference frame is right-handed, i.e., stars with $L_z < 0$ are in prograde orbits, while those with $L_z > 0$ are retrograde.
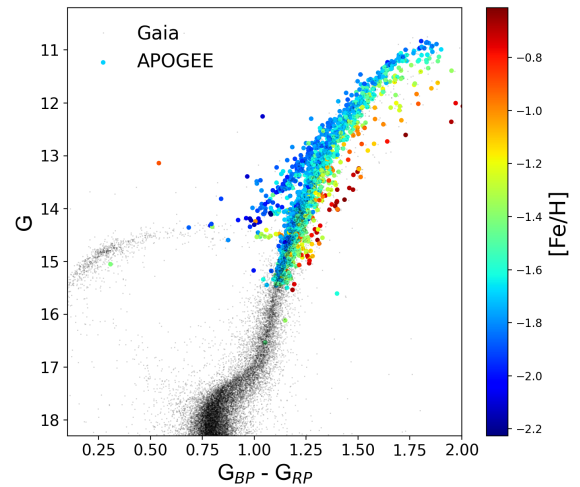

Figure 1. Gaia-based color–magnitude diagram of the ω Cen system, with the APOGEE targets marked, color-coded by the ASPCAP-derived [Fe/H]. APOGEE observations are covering the wide distribution of the ω Cen red giant branch stars and also the wide metallicity spread.

2.1. APOGEE Observations of the ω Centauri Core

If our goal is to find stellar debris far flung from the ω Cen core, we need to rely on stellar properties that are not only characteristic of the system but also conserved. Stellar chemical abundance patterns are a property characteristic of parent systems that (for the most part) is maintained by their constituent stars for most of their lives. Fortunately, the ω Cen core has received special attention in APOGEE-2 (F. A. Santana et al. 2021), and these observations can be used to look for APOGEE-based chemical patterns that define ω Cen.

Stars in the ω Cen core were observed as faint as $H = 13.5$. As is routine for APOGEE, the nominal minimum signal-to-noise (S/N) is 100; nevertheless, for the ω Cen data analyzed here, including commissioning data obtained before the instrument and observing procedures were fully optimized, the range of S/N spans 40 to 300. A total of 1872 ω Cen stars had APOGEE spectra that were successfully processed through the ASPCAP (A. E. García Pérez et al. 2016). For further information about the ω Cen targeting strategy we refer the reader to F. A. Santana et al. (2021).

Figure 1 shows a Gaia-based CMD of the system, with the APOGEE targets marked, color-coded by the ASPCAP-derived [Fe/H]. As may be seen by the wide distribution of the ω Cen RGB stars in the CMD and the APOGEE-based metallicity distribution function (MDF) of these stars shown in Figure 2, the APOGEE targets span the full range of ω Cen populations ($-2.3 <$ [Fe/H] < -0.5). This wide coverage ensures that we sample the diverse range of ω Cen chemistries. Those chemistries allow us to search for abundance signatures of ω Cen directly as measured by APOGEE. Some of the unusual chemical properties exhibited by ω Cen have been highlighted in S. Mészáros et al. (2020, 2021).

In Figure 2 we also show the [Fe/H] distribution of C. I. Johnson & C. A. Pilachowski (2010, "JP10"). There is excellent agreement between the APOGEE and JP10 [Fe/H] distributions, with 511 stars in common between the two samples. The figure also presents the histogram of discrepancies between the two independent measurements. The comparison indicates a strong agreement, with a minimal offset of 0.01 and a standard deviation of just 0.1. Although
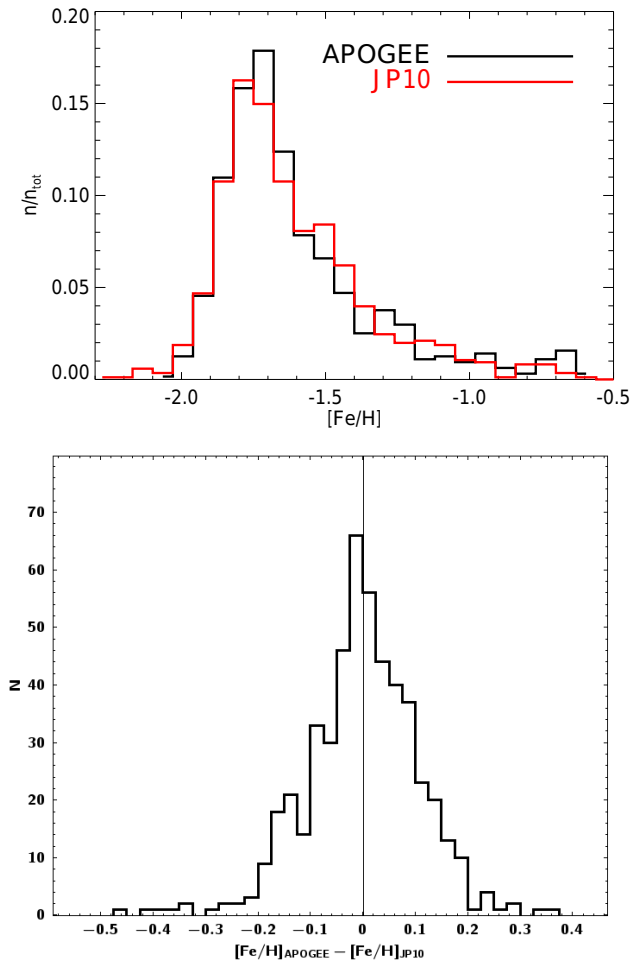
Figure 2. Top panel: Normalized fraction of the metallicity distribution function of ω Cen populations for the APOGEE (black) and C. I. Johnson & C. A. Pilachowski (2010, "JP10") (red) sample. There is an agreement between the APOGEE and JP10 [Fe/H] distributions. Bottom panel: Histogram of the discrepancies between the [Fe/H] measurements from APOGEE spectra and the values from JP10. The two independent measurements show good agreement, with a standard deviation of just 0.1.

every GC studied so far harbors at least two stellar generations distinct in chemical composition among the light elements (R. Gratton et al. 2004) and also age, GCs are still found to be mono-metallic objects as far as abundances of heavier elements are concerned.[18] The most notable exception is ω Cen, where evidence of several bursts of star formations with corresponding peaks in the metal abundance are reported (e.g., J. E. Norris & G. S. Da Costa 1995; C. I. Johnson & C. A. Pilachowski 2010; R. G. Gratton et al. 2011; S. Mészáros et al. 2021). In the next section, we discuss how we use the chemical peculiarities of ω Cen to identify debris candidates in the APOGEE survey.

3. ω Cen Debris Candidates

As discussed, GCs are known to display very uniform metallicities and prominent light element abundance correlations and anticorrelations. The most well-known of these are

---

[18] This is apart from a few notable confirmed exceptions: M54 (M. Bellazzini et al. 2008), M22 (A. F. Marino et al. 2009), and M2 (D. Yong et al. 2014). See Table 10 in A. F. Marino et al. (2015), for a summary of clusters with iron spreads.

the Na–O, Mg–Al, and C–N anticorrelations detected in most of the GCs analyzed so far (e.g., E. Carretta et al. 2009a, 2009b; E. Pancino et al. 2017). In the case of ω Cen, its unusual chemistry requires an evolution different from that followed by any known globular cluster. Previous studies show the complexity of the abundance pattern, together with its multiple populations (P. A. Denissenkov et al. 1998; E. Pancino et al. 2000; C. I. Johnson & C. A. Pilachowski 2010; R. G. Gratton et al. 2011; A. F. Marino et al. 2012; S. Mészáros et al. 2021), suggesting that ω Cen was massive enough to retain the ejecta of supernovae and the subsequent enrichment of new stellar generations with iron produced at the end of each burst of star formation. In principle, these distinct chemical signatures make GC stars stripped off their original cluster easily identifiable (e.g., S. L. Martell et al. 2016; R. P. Schiavon et al. 2017; D. Horta et al. 2021; S. G. Phillips et al. 2022, and references therein).

K. Freeman & J. Bland-Hawthorn (2002) discussed the concept of *chemical tagging*, in which stars are linked to individual star formation events when their abundance patterns in a range of elements, from α to Fe-peak, light to heavy s- and r-process, are the same (e.g., A. W. Mitschang et al. 2014). Chemical tagging techniques have already been explored using the APOGEE data set (e.g., D. W. Hogg et al. 2016; M. Ness et al. 2018; J. J. Andrews et al. 2019; J. J. Webb et al. 2020), and also the so-called *weak* chemical tagging, where we chemically label stars born in the same type of stellar system rather than the same unique stellar system (e.g., J. G. Fernández-Trincado et al. 2017; R. P. Schiavon et al. 2017; C. R. Hayes et al. 2018; S. Hasselquist et al. 2019).

In this section, we explain how we select debris candidates using *weak* chemical tagging from a neural network model that has the APOGEE ω Cen core as a training sample. We also explore the chemodynamical properties of the debris candidates.

3.1. Chemical Selection of Debris Candidates in the APOGEE Survey: Chemical Tagging Model

As a first step to identifying ω Cen candidates, we search for stars that share common patterns in their chemical abundances across a range of elements, in hopes that these so-called "chemical tags" are unique to the evolutionary origins of ω Cen (chemical tagging references). Instead of specifically modeling the numerous complex processes that underlie the chemical abundance patterns of ω Cen progenitors, we employ a black-box model capable of identifying arbitrary, potentially nonlinear relationships across a large number of dimensions. For this we use a "neural network" (e.g., J. Schmidhuber 2014). We built the training set using the ω Cen core observed by APOGEE (see Section 2.1 for details). We select the ω Cen stars for which the S/N exceeds 75 and no ASPCAPBAD and STARFLAG are set (J. A. Holtzman et al. 2015). This yields a total of 1794 objects for the training set. The same selection in terms of S/N and APOGEE flags is applied to the entire APOGEE sample. Figure 3 shows the distribution of six abundances used in the chemical tagging model for the training set (dashed red line), the model training data (solid black line), and the full APOGEE sample (gray line).

For our search for ω Cen tidal debris, we do not include focused APOGEE stars in science programs that target specific objects such as the Sgr dSph galaxy (S. R. Majewski et al. 2013; S. Hasselquist et al. 2019; C. R. Hayes et al. 2020), the Large and Small Magellanic Clouds (D. L. Nidever et al. 2020), numerous
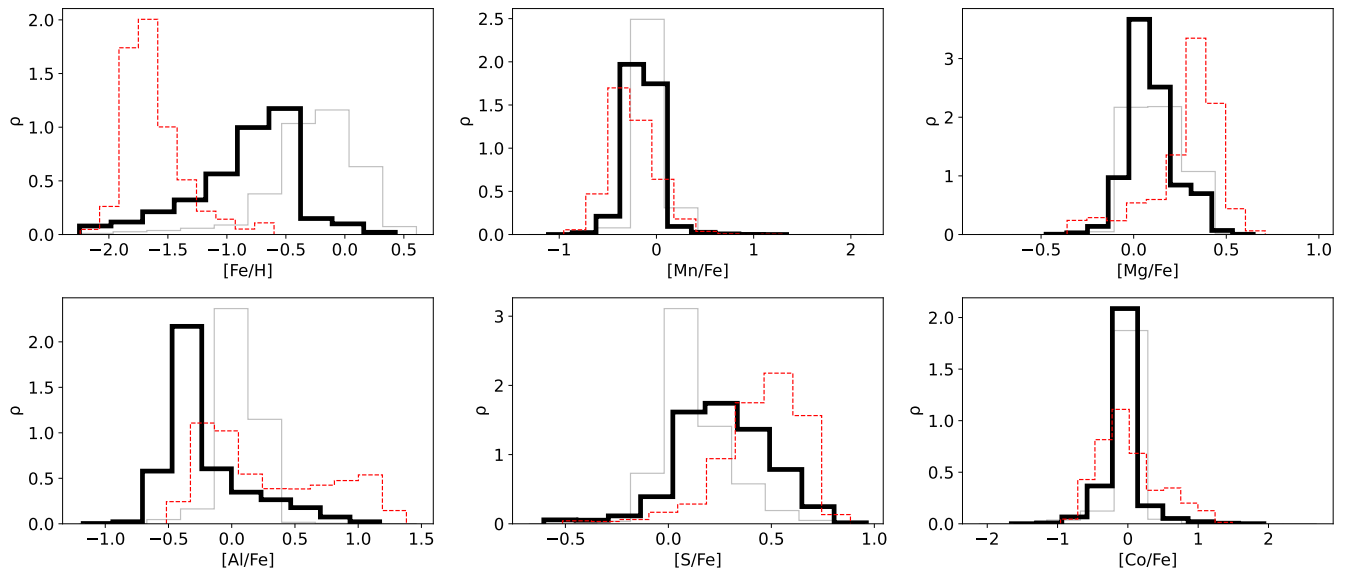
Figure 3. Distributions of the chemical tagging model negative training sample (solid black line), compared to the ω Cen subsample that represent the positive training data (dashed red line) and the full APOGEE sample (gray line) for six individual abundances.

star clusters different from ω Cen (S. Mészáros et al. 2020; R. P. Schiavon et al. 2024), and the dwarf spheroidal galaxy programs (G. Zasowski et al. 2017; R. L. Beaton et al. 2021; F. A. Santana et al. 2021) that are not germane to this study of field stars. To remove these specialized targets from our database, we identified the fields associated with the special programs and removed all the targets within those fields from our search database.

We perform the chemical tagging of candidate ω Cen debris by training a neural network model to generate a probability-like indicator of membership in ω Cen. Those stars determined by the model to be chemically similar to ω Cen have a higher value of this indicator, which can then be used to fine-tune the false positive rate of candidates in tagging. The neural network model we construct is of the well-known fully connected multilayer perceptron (MLP) type, having an input layer representing the abundance measurements, three hidden layers of neurons with 256, 128, and 32 units, respectively, and an output layer containing, in effect, a single unit representing the membership probability. Each edge is a transfer function $\omega x_{in} + \beta$, and each neuron applies an activation function $f(x)$ to its input and sums the results, which are then inputs to transfer functions of the next layer. For the two hidden layers, we use the Rectified Linear Unit (RelU) activation function, and for the final layer, we apply the *Softmax* function, which transforms the input to a probability of class membership, adding to 1 across the inputs. Training proceeds by computing the error on output for each training sample—where the error function used is the mean squared error—and adjusting the weights via a gradient descent technique so as to minimize the error.

To achieve a sufficient generalization of the model such that it could be used to tag unknown stars in our APOGEE sample, we need to train it with sufficient examples of both the target (ω Cen) and representative negative examples. We include 1454 stars from 27 known globular clusters present in our filtered APOGEE sample (R. P. Schiavon et al. 2024), in addition to 5434 stars from the LMC and the SMC (D. L. Nidever et al. 2020), and 400 identified as members of the Sagittarius dSph or stream (C. R. Hayes et al. 2020). We note that while the globular cluster sample provides negative

examples, there is also an expectation that these are chemically homogeneous to a higher degree than "field" stars and thus are more separable, leading to an overly optimistic view of performance if treated alone. The LMC, SMC, and Sgr stars provide a more well-mixed background with more complex enrichment histories built-in. These combined form the so-called negative sample that we use to train the chemical tagging model. In total we have 15,119 objects that comprise the negative sample.

The model is operating entirely in chemical space. Following the discussion described in J. A. Holtzman et al. (2018) and Abdurro'uf et al. (2022), we use the following individual abundances measured in the APOGEE spectra for our exercise: [C/Fe], [N/Fe], [O/Fe], [Mg/Fe], [Al/Fe], [Si/Fe], [Mn/Fe], [Ni/Fe], [Fe/H], [CI/Fe], [Na/Fe], [K/Fe], [Ca/Fe], [Co/Fe], and [Ce/Fe]. Of these, Mg, Si, Na, K, and Ca are derived in NLTE by the ASPCAP pipeline. To avoid introducing significant bias through the imputation of missing abundance measurements, we excluded any element for which the fraction of missing values in the negative sample differed by more than 25% points from that in the ω Cen sample. This exercise removed [Na/Fe] and [Ce/Fe] from the candidate abundances. Table 1 shows the final list of abundances used and coverage among the target and negative samples.

Figure 4 shows the performance of the model in terms of recall (the proportion of cluster stars that were correctly identified as such, the true positive rate) and precision (the proportion of positive labels that were correctly marked positive) as a function of threshold in probability ($P > P_{thresh}$). We use cross-validation. A random model—one that makes an uneducated guess for each input—would have a constant precision equal to the proportion of positive samples in the data set for all thresholds, while recall would increase linearly with decreasing threshold, achieving 1 and a threshold of 0 (simply assuming everything is a member).

3.2. Chemodynamical Study of Debris Candidates

Figure 5 shows the stellar APOGEE [Fe/H] as a function of ω Cen chemically tagged membership probability. In this figure, we

Table 1
Model Input Abundances Coverage

Sample	[Si/Fe]	[Fe/H]	[Mg/Fe]	[Ni/Fe]	[Al/Fe]	[O/Fe]	[Ca/Fe]	[CI/Fe]	[K/Fe]	[C/Fe]	[CO/Fe]	[N/Fe]	[Mn/Fe]
ω Cen	1.00	1.00	0.99	0.99	0.99	0.97	0.94	0.90	0.89	0.88	0.81	0.69	0.67
Negative	1.00	0.99	1.00	0.99	0.87	0.99	0.99	0.97	0.96	0.97	0.95	0.89	0.63
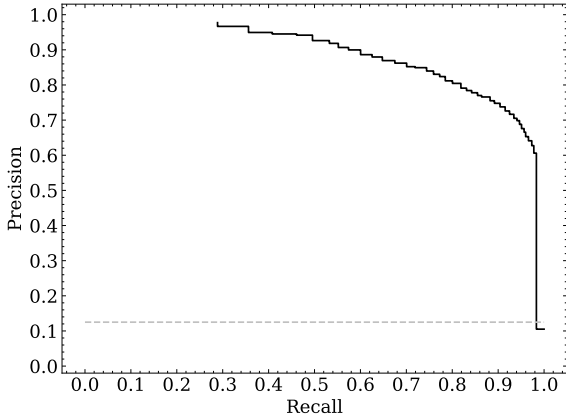
Figure 4. Neural network model performance. The best model recall and precision are plotted for $P > P_{\text{thresh}}$ from 0 to 1 at intervals of 0.01. The dashed gray horizontal line at 0.12 represents a random uneducated model. Our best fit does substantially better, achieving close to 80% recall at 80% precision.

Figure 5. [Fe/H] as a function of chemically tagged membership probability. Note the built-in dependence on [Fe/H] abundance and the resulting MW structure detected by the model. Also note the heavy tendency for low probabilities—more than 99% of stars in the sample have $P < 0.01$.

clearly detect the structure related to the MW disk and halo at very low probabilities. We also have a prominent overdensity close to $P \sim 1$ and ranging from $-2.1 < $ [Fe/H] $ < -1.2$. Interestingly, there is a very metal-poor "plume" ([Fe/H] < -2.0) with a $P \sim 0.1$ following the chemical space of ω Cen, but distinct from the remaining substructures identified in the figure.

We now explore the chemical abundance patterns for C+N,[19] the α-elements (O, Mg, Si, Ca), Al, Ni, and Ce for the ω Cen debris candidates (see Figure 6). For all of these exercises, the ω Cen core observed by APOGEE (see Section 2.1) is removed. For a detailed chemical abundance analysis ω Cen core stars using APOGEE abundances, we refer the reader to S. Mészáros et al. (2021) and A. C. Mason et al. (2025). We select these elements because they are among the most precise APOGEE abundances across the full parameter space covered here and are among the most accurate when comparing to optical studies (e.g., H. Jönsson et al. 2020; S. Hasselquist et al. 2021).

The data points representing ω Cen debris candidates in Figure 6 are color-coded by the ω Cen membership probability, where we show the debris candidates with $P > 0.8$. We find that the number of ω Cen debris candidates with $P > 0.8$ is 463, while for $P > 0.9$ we have 284 candidates and for $P > 0.95$ the total number is 186 objects. Table 2 shows the first four entries of the debris candidates with $P > 0.8$.

The results in Figure 6 show that there is an overlap, especially for O, Mg, Si, Ca, and Ni, between the multiple populations of the ω Cen debris candidates and the field stars in the Milky Way halo. This shows the efficiency of the neural network employed in this study (Section 3.1) to discern
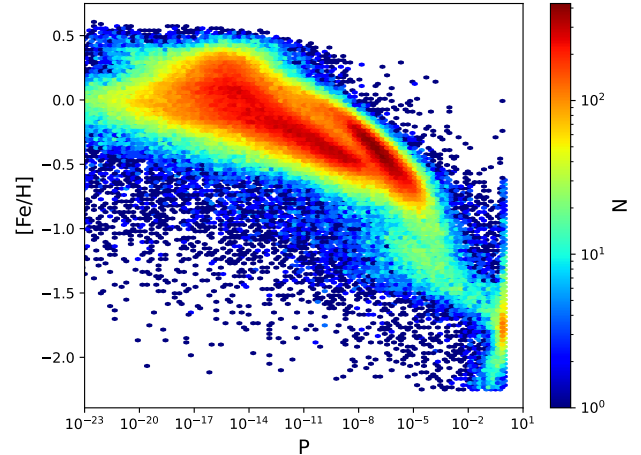
populations with different chemical evolution histories. A good number of the debris candidates are clearly enhanced in C+N, Al abundances with respect to the rest of the debris population and most of the Galactic halo. For instance, the high [Al/Fe] abundances we see in some globular cluster stars implies that a previous generation of higher-mass or evolved stars must have contributed to their chemical composition (C. Charbonnel & N. Prantzos 2006). We also see this *excess* in other light elements, like in the C+N panel. The hallmark C+N and Al trends are potential evidence that an extended part of the ω Cen tidal debris stream has been found.

Furthermore, we try to understand the optimal selection for ω Cen membership probability. Figure 7 shows the reverse Cumulative Distribution Function (CDF) for the ω Cen membership probability of ω Cen (black line) and four clusters for which APOGEE observed more than 200 individual members. It is remarkable how chemically unique all clusters are compared to ω Cen, despite a clear overlap in the overall metallicity distribution and in other elements, and also between them. The majority of clusters have an extremely low ω Cen membership probability. The red line in Figure 7 represents all globular cluster members observed by APOGEE DR17. Although the overwhelming majority of cluster members (>85%) have an extremely low probability of belonging to ω Cen, we determine that approximately 10% of the total members of other clusters could have a probability of 0.1 and only 1% a probability of 0.6 to be part of ω Cen. This exercise suggests that, to identify genuine ω Cen debris in the APOGEE sample, we should favor objects with probabilities greater than 0.6.

In the following sections, we analyze these populations in detail. Focusing on the substructure observed in Figure 5, we identify mainly five different populations in this APOGEE sample; what is commonly called the thin/thick disk, the

---

[19] We combine C and N because stars change their [C/Fe] and [N/Fe] abundances during dredge-up ascending to and along the giant branch, but these processes occur in such a way that the [(C+N)/Fe] abundance remains largely constant before and after these mixing processes (e.g., R. G. Gratton et al. 2000).
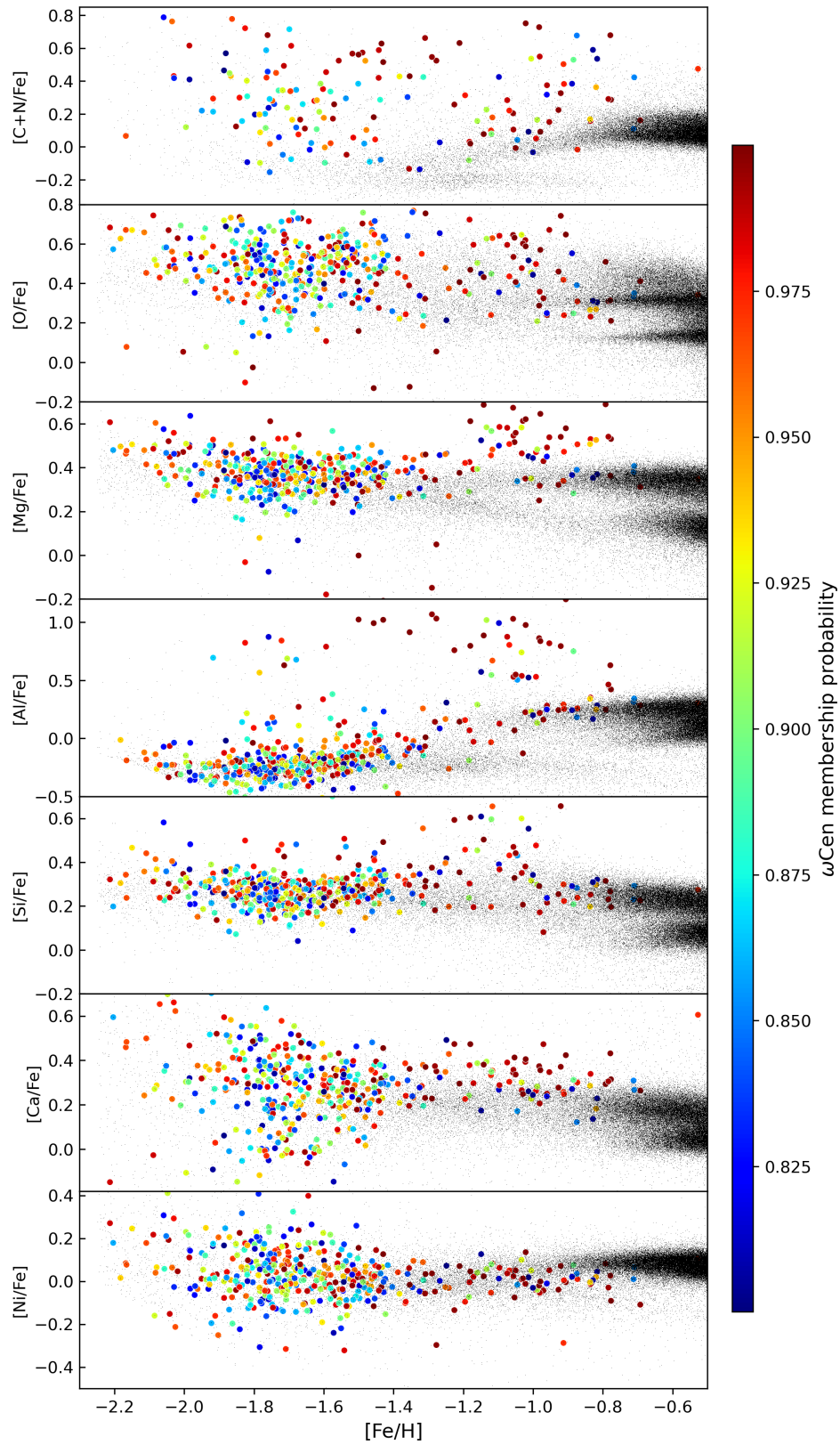
Figure 6. Chemical abundance patterns of select elements for ω Cen debris candidates as compared to the MW. The debris candidates are color-coded by the ω Cen membership probabilities, and we only show candidates where $P > 0.8$

Table 2
Column Descriptions for the ω Cen Debris Candidates

Column Name	Data Type	Description
target_id	String	Unique source identifier
apogee_id	String	APOGEE identifier for the star
C_FE	Double	Carbon-to-iron abundance ratio
N_FE	Double	Nitrogen-to-iron abundance ratio
O_FE	Double	Oxygen-to-iron abundance ratio
...	...	...
ra	Double	R.A.
dec	Double	Decl.
teff	Double	Effective temperature
logg	Double	log surface gravity
snrev	Double	S/N
pred_ocen	Double	ω Cen membership probability

Note. This table lists the metadata for the selected columns from the machine-readable version. It provides column names, data types, and brief descriptions for the parameters.

(This table is available in its entirety in machine-readable form in the online article.)

metal-weak thick disk (e.g., J. Norris 1986; H. L. Morrison et al. 1990; T. C. Beers et al. 2002; A. C. Robin et al. 2014; B. Anguiano et al. 2020), the halo component with a nonrotating average motion (e.g., M. Chiba & T. C. Beers 2000; C. R. Hayes et al. 2018), the abovementioned metal-poor "plume," and the ω Cen debris candidates close to $P \sim 1$.

3.2.1. Lindbland Diagram and Orbital Actions

The combination of chemical consistency with stellar kinematics can help to characterize the ω Cen tidal debris candidates together with the other substructures identified in this exercise. The classical Lindblad diagram (E–L_z) helps to identify circular orbits from the regions where the orbits are eccentric (e.g., J. A. Sellwood & M. Preto 2002). To further investigate the possible association of ω Cen debris candidates with the putative cluster, we explored orbital actions (J_R, J_ϕ, J_z). In axisymmetric potentials, they are integrals of motion and quantify the amount of oscillation of the star along its orbit in the Galactocentric (R, ϕ, z) direction, respectively. Furthermore, in an axisymmetric potential, the third action J_ϕ is the component of the angular momentum around the symmetry axis ($J_\phi \equiv L_z$). However, the identification of stellar debris in kinematic-related spaces should be treated with caution. For example, I. Jean-Baptiste et al. (2017) using high-resolution, N-body simulations, showed that caution must be employed before interpreting overdensities in any of those spaces as evidence of relics of accreted satellites. They showed that overdensities of multiple satellites overlap, and satellites of different masses can produce similar substructures. Therefore, reconstructing the ω Cen accretion event required careful chemical identification of candidates complemented by kinematic information (e.g., D. Horta et al. 2023).

We already discussed in Figure 5 the different substructures we found using a *weak* chemical tagging neural network model together with the *probability* to belong to ω Cen. We constructed the Lindblad diagram (energy E versus L_z) to investigate whether there is a kinematic connection between these substructures and the chemically selected ω Cen debris and the other clusters. The left-hand panel of Figure 8 investigates the region-dominated by a stellar population within $-1.9 < $ [Fe/H] < -0.9 and ω Cen membership probability smaller than 10%. The selected area is colored in orange for all panels. In blue we have the entire sample. The Lindblad diagram (left-hand middle panel) reveals at least three structures. A clean metal-poor population in prograde motion, very likely associated with the metal-weak thick disk (e.g., G. Cordoni et al. 2021). Another structure clearly visible in the diagram is a prominent nonrotating high-energetic population. It is widely accepted that this debris is dominated by a merger of a dwarf galaxy as the progenitor, now called "Gaia-Sausage-Enceladus (GSE)" (V. Belokurov et al. 2018; A. J. Deason et al. 2018; M. Haywood et al. 2018; A. Helmi et al. 2018; A. Fattahi et al. 2019). However, using APOGEE (S. R. Majewski et al. 2017) and GALAH surveys (G. M. De Silva et al. 2015), T. Donlon & H. J. Newberg (2023) have shown that the stellar populations in the local stellar halo are inconsistent with a scenario in which the inner halo is primarily composed of debris from a single massive, ancient merger event, as has been proposed to explain the GSE structure.

Finally, there is another nonrotating structure with low energy. D. Horta et al. (2021) claimed this population as a major building block of the halo buried in the inner Galaxy and called it *Heracles*. Nevertheless, it is relevant to point out that the Milky Way bulge also populates this area of the Lindblad diagram. Furthermore, the existence of bulge metal-poor stars has been reported (e.g., L. M. Howes et al. 2016; S. M. Wylie et al. 2021, and references therein). The right-middle panel in Figure 8 reveals the radial action J_R as a function of the orbital energy (E). The three components described above are also visible in this energy-action space; the metal-weak thick disk and the nonrotating low orbital energy population both show a low J_R. However, the accreted GSE structure has a large range and very high-J_R values compared to the other two main structures. V. Belokurov et al. (2018) showed that this debris has a strongly radial orbit that merged with the Milky Way at a redshift $z \leqslant 3$. All of these structures have a very low probability of being chemically associated to the core of ω Cen. The lower panel in Figure 8 shows the [Fe/H]–[Mg/Fe] plane and illustrates that the vast majority of disk stars are not part of the structures discussed above following the selection using the ω Cen membership probability and [Fe/H] derived from APOGEE spectra.

We now study the metal-poor "plume" on the right-hand panels of Figure 8. We select this population where ω Cen membership probability is smaller than 10% and where $-2.5 < $ [Fe/H] < -1.9 (see also Figure 5). The energy-action spaces in the middle panels suggest that this is a debris in the Milky Way halo with a very likely accreted origin. This debris, with both prograde and retrograde members and covering areas in these diagrams similar to GSE debris, is chemically independent of GSE from our weak chemical tagging exercise. R. P. Naidu et al. (2020) also reported a metal-poor high-α debris, selecting only a retrograde stellar component (l'itoi). Our findings suggest that the progenitor of this debris should be larger than previously reported, showing retrograde and also prograde motion, and probably an important building block of the MW halo.

We finally focus on the ω Cen debris candidates. Figure 9 shows the energy-action spaces for a population with $P > 0.8$. Following the Lindblad diagram, some of the debris have prograde and retrograde disk-like kinematics, whereas most of the debris lies within the accreted halo, showing high-J_R
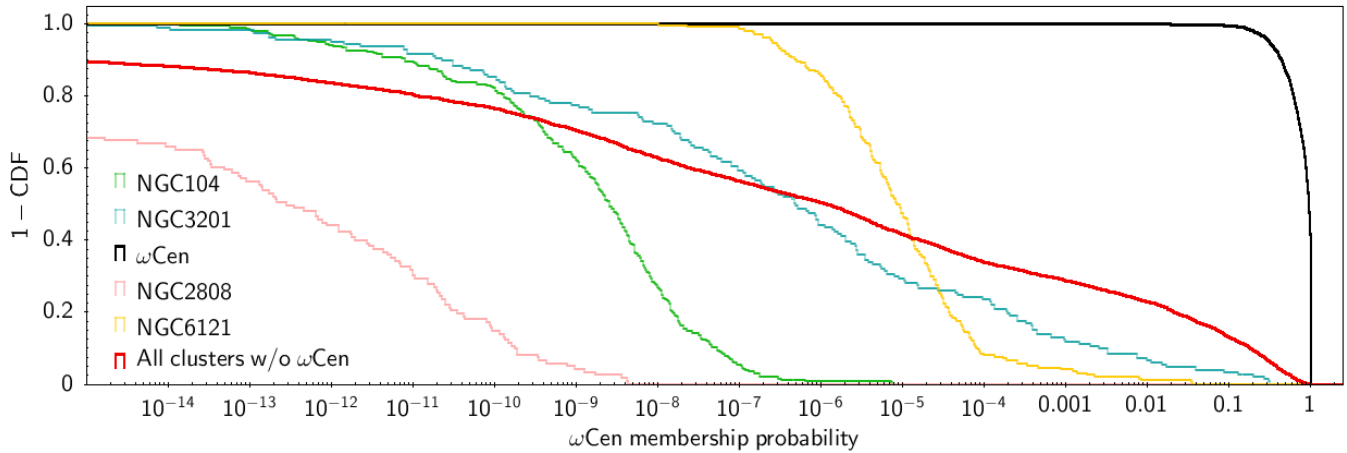
Figure 7. Inverse cumulative distribution functions for the ω Cen membership probability for four distinct clusters (NGC 104, NGC 3201, NGC 2808, and NGC 6121), as well as ω Cen itself (black line). We also present the CDF for every member of the globular cluster listed in APOGEE DR17, excluding the ω Cen members. Although 90% of the members of other groups have an extremely low probability of being part of ω Cen (red line), according to our chemical selection, approximately 10% of the total of members of other clusters could have a probability of 0.1, and only 1% a probability of 0.6 to be part of ω Cen.

values. We notice that GSE, the metal-poor "plume" and the ω Cen debris candidates show a very similar energy-action space behavior. While they are all part of the accreted halo, they are chemically distinct from our chemical tagging exercise, suggesting that they are independent events that build up the Milky Way stellar halo. However, ω Cen exhibits evidence of chemical enrichment and could be the innermost part of the progenitor system. Hence, the chemical tagging performed in this study cannot definitely say that GSE and ω Cen have distinct origins. In the next section, we explore a few orbital parameters of the ω Cen debris candidates in more detail.

3.2.2. Orbital Parameters

Using the selected populations described in the previous section, where we used the ω Cen membership probability and [Fe/H], we investigate the stellar eccentricity, vertical excursion from the Galactic plane (Z_{max}) and apocenter (R_{apo}).

The top panels in Figure 10 show the maximum height achieved above the Galactic plane Z_{max} versus the orbital eccentricities for $P < 0.1$ (left) and $P > 0.8$ (right), respectively. For the stellar population where $-1.9 < $ [Fe/H] $ < -0.9$ and ω Cen membership probability is smaller than 10%, we find a group with high orbital eccentricity ($e > 0.8$), that also tends to have larger vertical excursions. These populations are associated with GSE. The low orbital eccentricity population is a mixture of different origins, possible remnants of accretion events, the metal-weak thick disk, and the MW bulge (e.g., J. T. Mackereth et al. 2019; A. B. A. Queiroz et al. 2021) There is also an apocenter pile-up (see bottom left panel in Figure 10), in both the sample of stars with high and low orbital eccentricities. A. J. Deason et al. (2018) suggested a massive dwarf progenitor, especially for the high eccentricity sample.

The star associated with ω Cen debris for a $P > 0.8$ show a wide range of Z_{max} ($0.5 < Z_{max} < 100$ kpc), together with a large range in eccentricity ($0.1 < e < 1.0$). In Figure 10 we also have the position of ω Cen core marked as a red cross ($e \sim 0.6$, $Z_{max} \sim 2$ kpc).

4. Is ω Centauri the Stellar Nucleus of the GSE Galaxy?

G. C. Myeong et al. (2018) reported the properties of eight GCs, including ω Cen, that are consistent with being associated

with the merger event that gave rise to the GSE. Furthermore, D. Massari et al. (2019) and J. Pfeffer et al. (2021) further suggested that ω Cen could be the surviving nuclear star cluster of GSE. D. A. Forbes (2020) assigned NGC 1851 as the nuclear star cluster of GSE, and ω Cen with Sequoia (G. C. Myeong et al. 2019). G. Limberg et al. (2022) estimated the stellar mass of the progenitor of ω Cen to be $M \approx 1.3 \times 10^9 \ M_\odot$, well within literature expectations for GSE. This leads the authors to envision GSE as the best available candidate for the original host galaxy of ω Cen. Note that T. Donlon & H. J. Newberg (2023) reported that the structure called the GSE is not really a single ancient massive merger; they found that it is instead built up from a combination of many smaller merger events.

In this section, we use the ω Cen debris candidates identified in this study to further understand its progenitor and its possible association with the structure reported in the Milky Way halo.

4.1. Building a GSE Candidate Sample

Creating a pure GSE sample that is free from contamination by other structures is challenging. A. Carrillo et al. (2024) explored selections made in eccentricity, energy-angular momentum (E–L_z), radial action-angular momentum (J_r–L_z), action diamond, and [Mg/Mn]-[Al/Fe] in the observations, see also D. Horta et al. (2023). In all these selections, they reported contamination from in situ and other accreted stars.

For the purpose of this study, we use the parent sample of the GSE defined in D. Horta et al. (2023), based on the (E–L_z) plane. Note that a good number of ω Cen debris and the metal-poor "plume" are also within this selection. We stress that there is no guarantee that this selection of GSE provides an unbiased sample of the stars of the accreted galaxy (e.g., D. K. Feuillet et al. 2020; P. Bonifacio et al. 2021).

Figure 12 shows the reverse cumulative distribution function of the ω Cen membership probability for the selected GSE members and ω Cen cluster, and on the right panel, the (E–L_z) plane for ω Cen debris candidates with $P > 0.8$ (red points) and the parent sample of the GSE (black points). The potential contamination from the metal-poor "plume" and the ω Cen is evident in the GSE selected sample for $P > 0.001$. Almost all GSE stars in our sample have a ω Cen membership probability

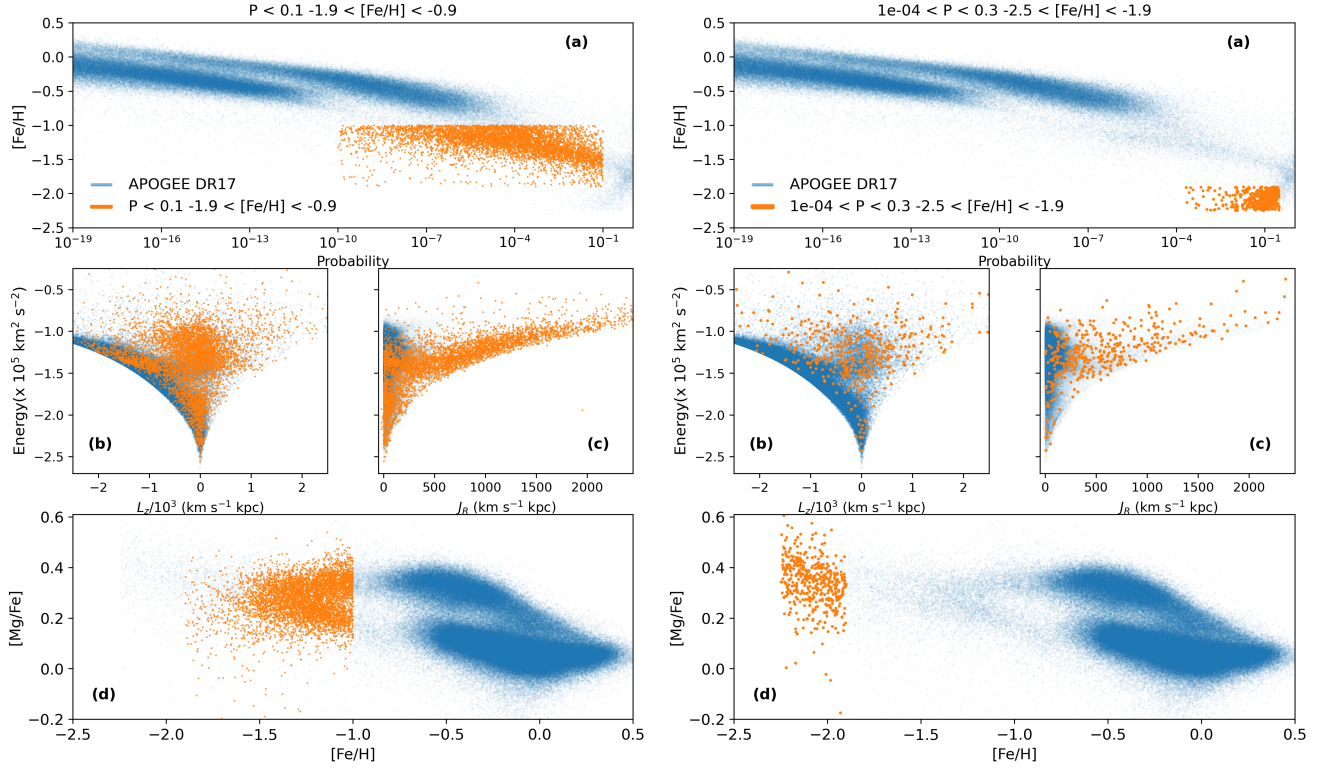**Figure 8.** ω Cen membership probability as a function of [Fe/H], energy-action spaces and the [Fe/H] - [Mg/Fe] plane. Left-hand panels: the orange color in these panels highlights the selection of $P < 0.1$ and $-1.9 <$ [Fe/H] < -0.9. There are clearly three structures, a metal-weak thick disk, a nonrotating low orbital energy population, and the halo debris associated with GSE. We discuss them in detail in the text. Right-hand panels: the orange color represents the selection for the metal-poor "plume," which is very likely an ancient merger in the MW halo. In all the panels, the blue data represent the APOGEE DR17 catalog. The figure helps visualize the chemodynamical study of the different structures identified in this study.
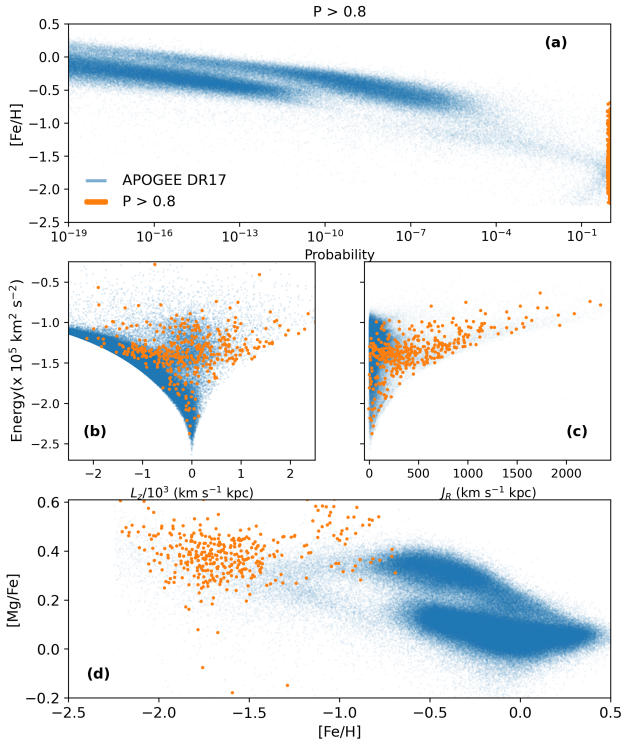
Figure 9. ω Cen membership probability as a function of [Fe/H], energy-action spaces and the [Fe/H]– [Mg/Fe] plane for the ω Cen debris candidates with $P > 0.8$. The Lindblad diagram reveals that most of the debris lies within the accreted halo with some having disk-like kinematics.

smaller than 0.1. Our results indicate that the selected GSE members are chemically distinct from the current ω Cen core, and hence the ω Cen debris identified in this study. We would expect a similar chemical evolution enrichment history for a large number of GSE members, as the progenitor galaxy and the putative cluster and its debris. However, it is well established that ω Cen shows clear signs of its own self-enrichment, e.g., GC-like chemical evolution producing large anticorrelations (E. Carretta 2019; D. A. Alvarez Garay et al. 2022). In fact, D. Romano et al. (2007) showed that in a closed-box self-enrichment scenario, the MDF of the clusters cannot be reproduced. However, the main chemical properties of ω Cen are matched if it is the compact remnant of a dwarf spheroidal galaxy that evolved in isolation and then accreted by the MW. D. Romano et al. (2007) assumed a relatively long-lasting star formation activity (though with most of the stars forming within 1 Gyr), standard IMF and standard stellar yields, their models satisfactorily reproduce several observed abundance ratios as a function of [Fe/H], proving that the ingested satellite would also have similar chemical properties to ω Cen. To make this scenario even more intricate, the GSE sample could be the product of many smaller mergers with a wide range of dynamical times (e.g., T. Donlon & H. J. Newberg 2023; T. Donlon et al. 2024).

4.2. M54 + Sgr = ω Cen?

Hubble Space Telescope photometry of the massive M54 cluster shows multiple turnoffs coming from the cluster population and Sgr, indicating different star formation epochs (M. H. Siegel et al. 2007). In this regard, E. Carretta et al. (2010)
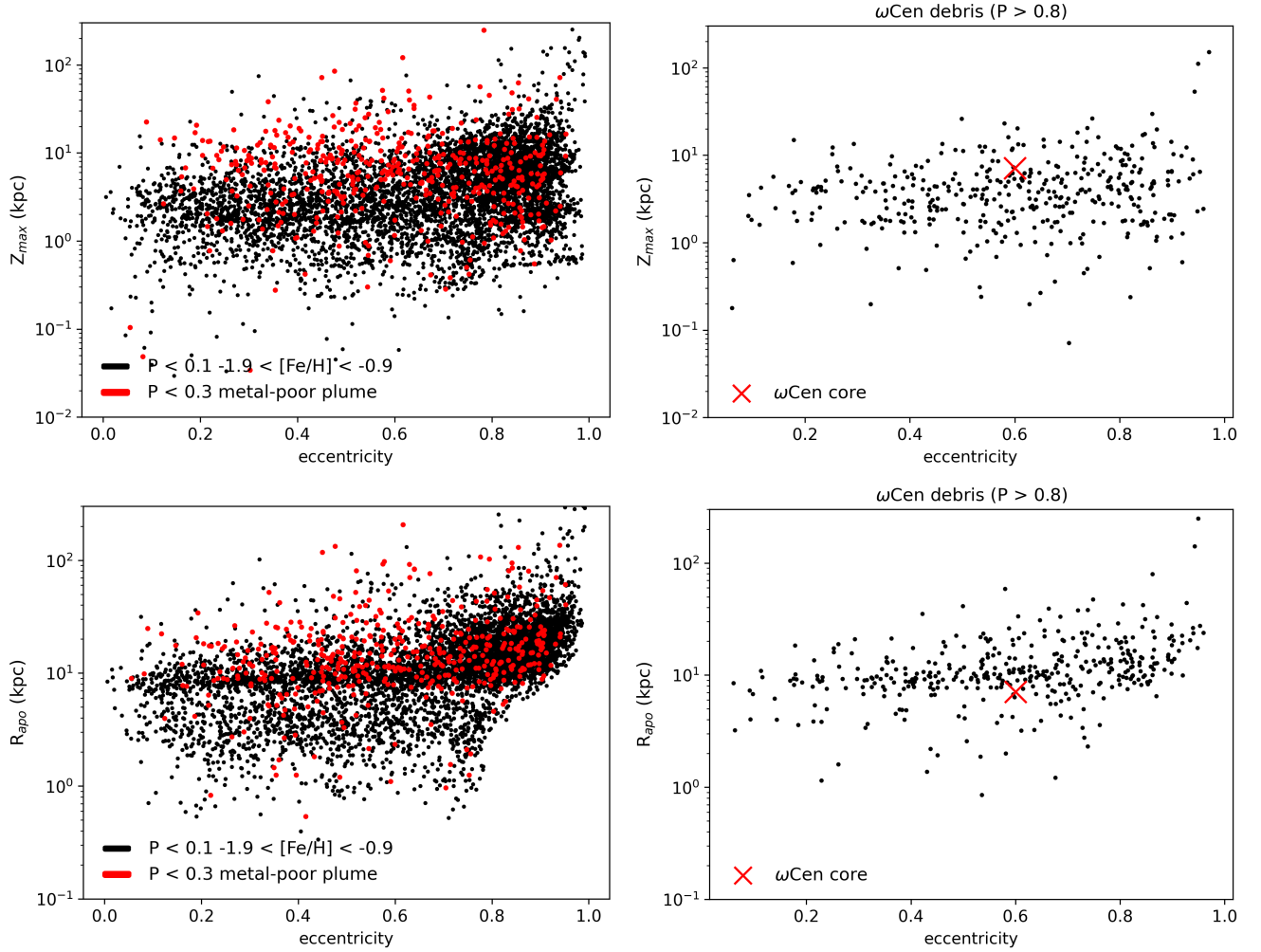
Figure 10. In the top panels we have the maximum height achieved above the Galactic plane Z_{max} vs. the orbital eccentricities for $P < 0.1$ and $-1.9 <$ [Fe/H] < -0.9 (left) and $P > 0.8$ (right), where ω Cen core is marked with a red X. The lower panel also shows the apocenter with respect to the eccentricity. See the text for details.

found that by including stars of the Sgr nucleus in their M54 spectroscopic sample, the metallicity distribution is similar to that observed in ω Cen. E. Carretta et al. (2010) concluded that M54 and ω Cen are nuclear clusters in dwarf galaxies showing a different phase of their dynamical evolution.

Following this idea, we performed a similar training and probability estimation as described for ω Cen but now trained in M54 APOGEE members (R. P. Schiavon et al. 2024) and left the APOGEE Sgr stream objects (C. R. Hayes et al. 2020) out of the negative sample. Our goal is to see what fraction of Sgr stars are chemically tagged to M54. As we described in Section 3.1, Figure 11 shows the performance of the model in terms of recall (the proportion of cluster stars that were correctly identified as such—the true positive rate) and precision (the proportion of positive labels that correctly marked positive). Figure 11 indicates that the model is not good at differentiating M54, therefore any predictions would not be meaningful.

There are a large number of pieces of evidence that relate the M54 cluster to Sgr dSph (e.g., A. C. Layden & A. Sarajedini 2000; M. H. Siegel et al. 2007; M. Bellazzini et al. 2008).
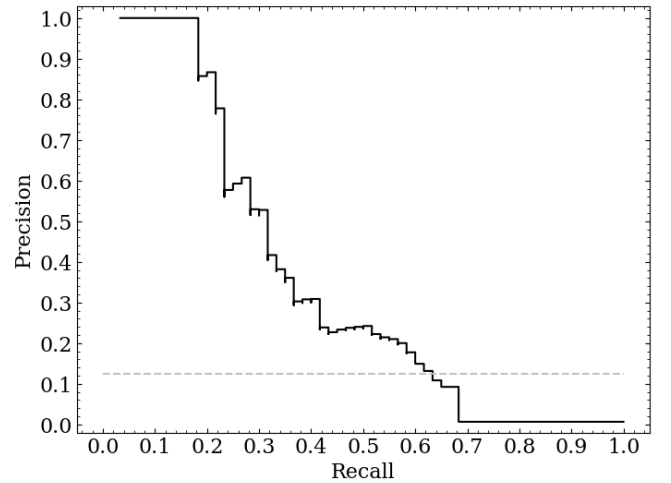
Figure 11. Best model recall and precision are plotted for $P > P_{thresh}$ from 0 to 1 at intervals of 0.01. The dashed gray horizontal line at 0.12 represents a random uneducated model. The model is not helpful at discriminating M54, therefore any predictions would not be meaningful.
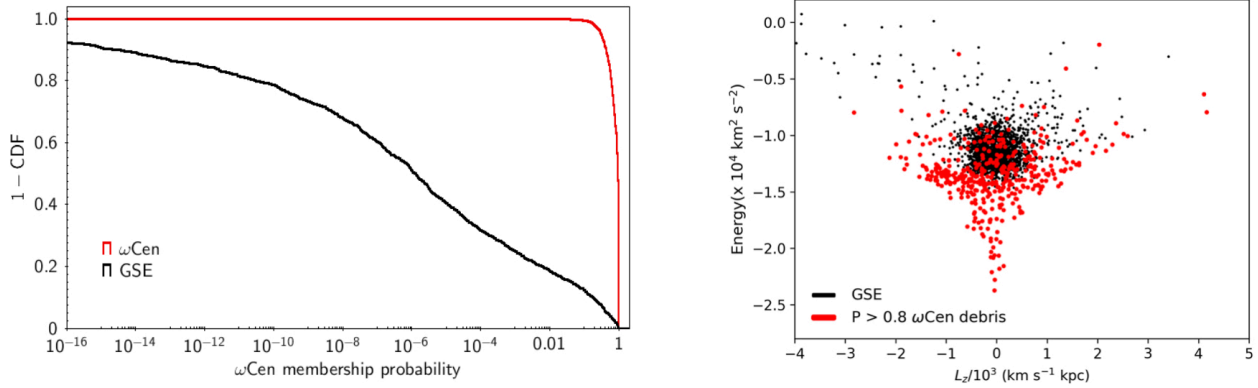
Figure 12. Left panel: Reverse cumulative distribution functions for the ω Cen membership probability for the selected GSE sample (blue line) and the ω Cen members (green line). Note the "bump" in the GSE sample for $P > 0.001$, those are ω Cen debris members and the metal-poor plume that made it into the GSE selection. More than 90% of the GSE members have a $P < 0.1$ to have a similar chemical pattern as the ω Cen cluster. Right panel: Lindblad diagram for the selected GSE sample (black dots) and the ω Cen debris candidates (red dots). The kinematical overlap between the different structures is not evident. Furthermore, the selected GSE sample do not show stars at low energy.

However, in this study, we found that our neural network modeling (see Section 3.1) is not able to chemically associate the core of M54 with those objects that are part of the Sgr stream, suggesting that most of the stars in the progenitor galaxy do not show the same chemical properties as M54. However, M54 APOGEE sample is potentially contaminated from the main body of the Sgr dSph. Additionally, C. R. Hayes et al. (2020) demonstrated the presence of a chemical composition gradient in the Sgr dSph, suggesting that even the galaxy's main body may not align with its streams.

4.3. Orbital Parameters

In this section, we study the kinematical structure of the parent sample of the candidates for the GSE (D. Horta et al. 2023) and the ω Cen debris candidates using the Lindblad diagram. *N*-body simulations show that a massive disk galaxy merging with the MW can generate debris with a complex phase-space structure, a large range of orbital properties, and a complex range of chemical abundances (Á. Villalobos & A. Helmi 2009; I. Jean-Baptiste et al. 2017; H. H. Koppelman et al. 2020).

In the right panel of Figure 12 we have the resulting angular momentum—orbital energy distribution for the GSE sample (black dots) and ω *Cen* debris candidates (red dots). Most of the ω Cen debris tend to pile up in a narrow range of Energy with a large angular momentum range. We also have debris candidates with low energy values and nonrotating kinematics. A comparison with the GSE sample needs to be made carefully, as this sample was selected using the (E–L_z) plane, hence biasing kinematically the sample. Figure 12 shows that the high energy ω *Cen* debris share similar angular momentum values with the GSE sample. However, our results indicate that there is no clear chemical and kinematical overlap between the ω *Cen* debris and the GSE sample.

5. Numerical Simulation Predictions

In this section, we study the predictions of the tidal disruption of the ω Cen progenitor using an *N*-body simulation. In particular, we discuss the global distribution of the components stripped by the tidal effects, and we compare the position and kinematics of the ω Cen debris identified in this study with the orbital motion of the progenitor derived in the simulations. ω Cen has singular characteristic, and there is evidence that ω Cen may be the remnant of a heavily stripped dwarf galaxy, as described in detail in Section 1. A detailed modeling of its progenitor remains challenging, mainly due to the difficulty of simulating the long-term orbital evolution and being able to mimic the current orbital elements of the cluster, as the evolution of the Galactic gravitational potential and the effect of dynamical friction are not negligible (e.g., A. Meza et al. 2005).

5.1. Methodology

In this study, we focus on the global distribution of the tidally stripped stars using a simple progenitor model. We first integrated the orbit backward in time in the MW gravitational potential from the current position of ω Cen using a test particle. We recovered the position and velocity of the cluster 500 Myr ago. The apocentric and pericentric distances are 7.1 kpc and 1.6 kpc, respectively, and it has experienced five pericentric passages over the last 500 Myr. During this time, we have assumed that the Galactic potential does not change with time. We then simulate the tidal disruption of a progenitor cluster using an *N*-body simulation. We construct the progenitor dwarf galaxy as a Plummer model using MAGI (Y. Miki & M. Umemura 2018). The total mass and scale radius of the Plummer distribution are set to $10^8 M_\odot$ and 1 kpc, respectively. We assume that the dark matter halo of the progenitor galaxy has already been stripped at the beginning of the simulation. The total number of particles is 1,048,576, and we use the gravitational octree code GOTHIC (Y. Miki & M. Umemura 2017) to run the simulation using the accuracy parameter of $\theta = 0.5$. We adopt the Plummer softening parameter of 16 pc.

5.2. Results

Figures 13 and 14 show the simulated distribution of ω Cen debris. The overplotted cyan points indicate the ω Cen membership candidates where $P > 0.8$. The tidally stripped ω Cen debris obtained from the simulation covers the spatial distribution of the observed ω Cen candidates. In addition, our simulation nicely reproduces the extent of the distribution of the candidates in terms of distance, proper motion, and radial velocity. The number density of debris is high around $(l, b)=(270°, -30°)$; that area is where APOGEE observed the TESS CVZ (R. L. Beaton et al. 2021; F. A. Santana et al. 2021). Multiple ω Cen candidates are
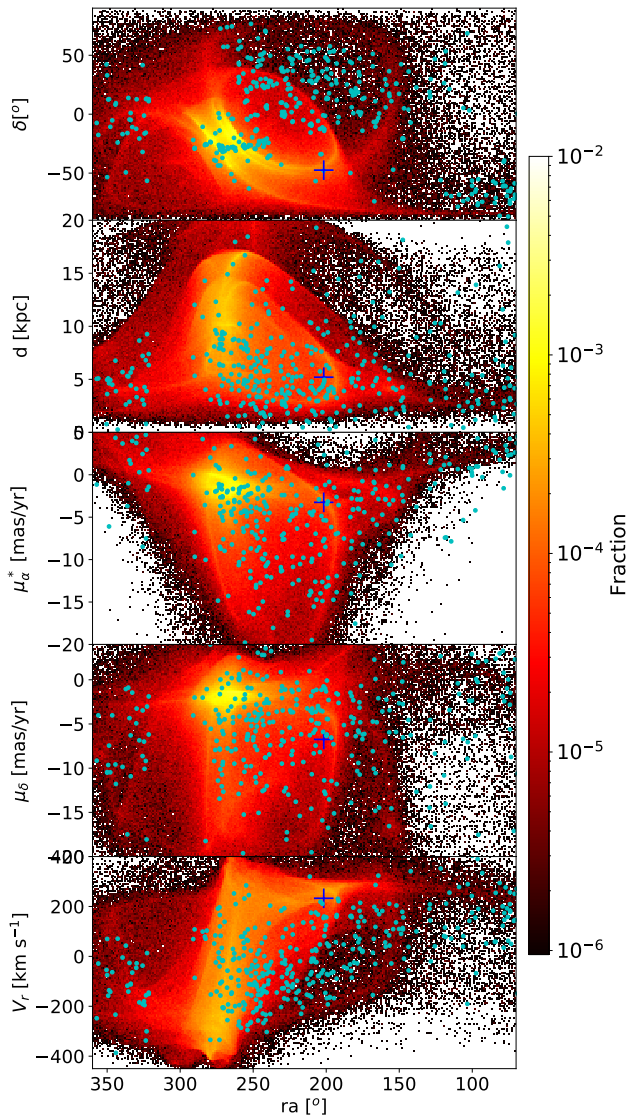
Figure 13. Distribution of the simulated ω Cen debris in (a) decl., (b) heliocentric distance, proper motion in (c) α and (d) δ, and (e) radial velocity as a function of α. The colors represent the mass fraction in each region normalized by the total mass of the ω Cen progenitor. The cyan points indicate the ω Cen membership candidates where the $P > 0.8$. The blue cross indicates the observed information of the ω Cen cluster.

Figure 14. Distribution of the simulated ω Cen debris in (a) Galactic latitude, proper motion in (b) α and (c) δ, (d) heliocentric distance, and (e) heliocentric velocity as a function of Galactic longitude. The colors represent the mass fraction in each region normalized by the total mass of the ω Cen progenitor. The cyan points indicate the ω Cen membership candidates where the $P > 0.8$. The blue cross indicates the observed information of the ω Cen cluster.

present along high-density streams. Beyond 10 kpc, the APOGEE data are poor. Therefore, it is acceptable that there are few ω Cen candidates in this region, even though we can see several structures derived from ω Cen in the simulation. The number density of ω Cen debris is high around $(ra, d) = (260°, 15\,\text{kpc})$, which could be a target for future observations of ω Cen tidal debris. Multiple streams around ω Cen, indicated by the blue plus, appear in the simulation. However, it should be noted that the APOGEE data around the ω Cen are not sufficient. In particular, the regions $120° < ra < 250°$ and $\delta < -10°$ have few APOGEE data. In addition, the streams have a large spread in proper motions, making it challenging to find the structure simply from the Gaia observations. For the regions of $100° < ra < 250°$ and $\delta > -10°$, the mass fraction of debris in the simulation is relatively small, while the ω Cen candidates are numerous. This is likely due to the richness of the APOGEE data in this region and the relatively close distances to the debris. It suggests that a large amount of ω Cen debris is still hidden.

The left panel of Figure 15 shows the Lindblad diagram for the simulated ω Cen debris, and in this figure we can also see that the tidal debris is distributed over a wide range in L_z. The major population has a retrograde orbit, but some debris has prograde kinematics. Although the integration time is slightly short, we also find an overdensity in the E–L_z plane. This overdensity lies in a similar or slightly lower energy region as the GSE (see right panel in Figure 12). It should be noted that the relics of multiple accreted satellites may appear in similar positions in the E–L_z plane, as pointed out by I. Jean-Baptiste et al. (2017). Hence, our approach with chemical tagging is powerful in approaching the origin of the substructures. The right panel of Figure 15 shows the radial action as a function of orbital energy. In addition to the E–L_z distribution, the simulated distribution of tidal debris in the E–J_R plane matches the scatter on the observed data. The ω Cen debris shows high J_R values, indicating that the debris has strong radial orbits.
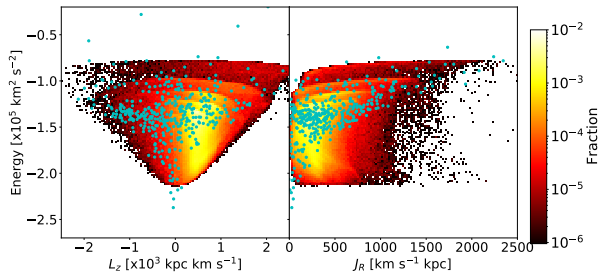
Figure 15. Left panel: the distribution of the ω Cen debris in the Lindblad diagram. Right panel: the distribution in the energy-action space. The cyan points indicate the ω Cen membership candidates where the $P > 0.8$.

According to ω Cen debris candidates obtained using the characteristics of the chemical abundance patterns, we find a nonnegligible prograde-orbiting stars (see Figure 9). The wide distribution on the L_z-axis requires that when the progenitor passes through the pericenter, a part of the progenitor has to pass on the opposite side of the Galactic center to the main component. For our adopted gravitational potential (J. Bovy 2015), the pericentric distance is about 1 kpc; therefore, a progenitor model with a radius of more than 1 kpc is required to obtain a broad distribution on the L_z-axis. Concerning the ratio of prograde to retrograde components, this suggests a strong dependence on the size of the progenitor and its density profile. In fact, a simulation with the current ω Cen-like progenitor (with a stellar mass of $10^6 M_\odot$ and a core radii of 76 pc) produces a distribution concentrated in the $L_z > 0$ region. Indeed, we cannot rule out the possibility that there have been periods of extremely small pericentric distances as a result of the time evolution of the Galactic potential. However, it should be emphasized that it becomes more difficult for the ω Cen core to survive in such cases. That is, the presence of a prograde component suggests that the progenitor was a dwarf galaxy with a somewhat large stellar mass ($\gtrsim 10^8 M_\odot$).

6. Summary and Conclusions

In this study we use data from the APOGEE survey S. R. Majewski et al. (2017) included in the SDSS Data Release 17 (DR17, Abdurro'uf et al. 2022). We also exploit Gaia DR3 (Gaia Collaboration et al. 2023), and the APOGEE StarHorse value-added catalog (A. B. A. Queiroz et al. 2020). A total of 1872 stars in the core of ω Cen have APOGEE spectra (F. A. Santana et al. 2021; S. Mészáros et al. 2021). Having the stellar individual abundances of the ω Cen core as a training sample and using chemical tagging from a neural network modeling we identify ω Cen debris candidates in the APOGEE survey. We test our neural network modeling using four different clusters observed with APOGEE containing more than 200 individual objects, those are NGC 104, NGC 3101, NGC 2808, and NGC 6121. Despite the clear overlap in metallicity and in other elements between ω Cen and these clusters, the model is able to show how chemically unique every cluster is with respect to ω Cen. Stellar members of these clusters have a very low ω Cen membership probability. We found 463 ω Cen debris candidates with a probability $P > 0.8$. Remarkably, we reported that a good number of them show C + N, Al, and Ce abundances enhanced with respect to other debris candidates and most Galactic halo stars.

A chemodynamical study of ω Cen debris candidates shows that most of them lie within the accreted MW halo; however, debris with prograde and retrograde disk-like kinematics is also

found. Most of the debris also has high radial action values. D. Massari et al. (2019) and J. Pfeffer et al. (2021) suggested that ω Cen was the nuclear star cluster of GSE. To further investigate this potential association we have compared the APOGEE parent sample of the GSE defined in D. Horta et al. (2023) with ω Cen. We found that nearly all the GSE stars in our sample show a ω Cen membership probability smaller than 0.1. This result indicates that the actual ω Cen core and the selected GSE members are chemically distinct. However, ω Cen shows clear evidence of its own self-enrichment, hence, the stars in its progenitor galaxy should have a different chemical evolution than the one we observe today in the core of ω Cen.

Despite the negative result associating GSE and ω Cen via chemical tagging modeling, we cannot rule out their potential association. The kinematical exercise findings are inconclusive as well; however, most of the ω Cen debris found in this study using stellar individual abundances lie in a different area covered by the GSE sample. There is some overlap with the GSE sample, but this is likely due to contamination from the ω Cen debris, as avoiding the GSE's influence when selecting any halo sample is nearly impossible. We also found a metal-poor "plume" with [Fe/H] < -2.0 in the probability—metallicity plane (see Section 2). This population has low probability of following the chemical pattern of ω Cen but it is distinct from the other structures like GSE. The energy-actions diagram shows that this population is very likely accreted and probably part of an important building block of the MW halo.

Finally, we have compared our observational results with the tidal disruption of the ω Cen progenitor using N-body simulations. We found that the properties of the debris from the simulations span the spatial distribution of the observed ω Cen candidates. Furthermore, the N-body simulation results suggested the progenitor was a dwarf galaxy with a somewhat large stellar mass ($\gtrsim 10^8 M_\odot$).

ORCID iDs

Borja Anguiano https://orcid.org/0000-0001-5261-4336
Arik W. Mitschang https://orcid.org/0000-0001-9239-012X
Takanobu Kirihara https://orcid.org/0000-0001-6503-8315
Yutaka Hirai https://orcid.org/0000-0002-5661-033X
Danny Horta https://orcid.org/0000-0003-1856-2151
Sten Hasselquist https://orcid.org/0000-0001-5388-0994
Ricardo P. Schiavon https://orcid.org/0000-0002-2244-0897
Steven R. Majewski https://orcid.org/0000-0003-2025-3147
Andrew C. Mason https://orcid.org/0000-0003-1502-2088
Adrian M. Price-Whelan https://orcid.org/0000-0003-0872-7098
Carlos Allende Prieto https://orcid.org/0000-0002-0084-572X
Verne V. Smith https://orcid.org/0000-0002-0134-2024
Katia Cunha https://orcid.org/0000-0001-6476-0576
David L. Nidever https://orcid.org/0000-0002-1793-3689

References

Abdurro'uf, Accetta, K., Aerts, C., et al. 2022, ApJS, 259, 35
Allende Prieto, C., Beers, T. C., Wilhelm, R., et al. 2006, ApJ, 636, 804
Alvarez Garay, D. A., Mucciarelli, A., Lardo, C., Bellazzin, M., & Merle, T. 2022, ApJL, 928, L11
Andrews, J. J., Anguiano, B., Chanamé, J., et al. 2019, ApJ, 871, 42
Anguiano, B., Majewski, S. R., Hayes, C. R., et al. 2020, AJ, 160, 43
Anguiano, B., Zucker, D. B., Scholz, R. D., et al. 2015, MNRAS, 451, 1229
Astropy Collaboration, Price-Whelan, A. M., Lim, P. L., et al. 2022, ApJ, 935, 167
Beaton, R. L., Oelkers, R. J., Hayes, C. R., et al. 2021, AJ, 162, 302
Beers, T. C., Drilling, J. S., Rossi, S., et al. 2002, AJ, 124, 931
Bekki, K., & Freeman, K. C. 2003, MNRAS, 346, L11
Bellazzini, M., Ibata, R. A., Chapman, S. C., et al. 2008, AJ, 136, 1147
Bellini, A., Bedin, L. R., Piotto, G., et al. 2010, AJ, 140, 631
Belokurov, V., Erkal, D., Evans, N. W., Koposov, S. E., & Deason, A. J. 2018, MNRAS, 478, 611
Blanton, M. R., Bershady, M. A., Abolfathi, B., et al. 2017, AJ, 154, 28
Bonifacio, P., Monaco, L., Salvadori, S., et al. 2021, A&A, 651, A79
Bovy, J. 2015, ApJS, 216, 29
Brown, A. G. A., Vallenari, A., Prusti, T., & de Bruijne, J. H. J. 2018, A&A, 616, A1
Buder, S., Sharma, S., Kos, J., et al. 2021, MNRAS, 506, 150
Calamida, A., Zocchi, A., Bono, G., et al. 2020, ApJ, 891, 167
Carraro, G., & Lia, C. 2000, A&A, 357, 977
Carretta, E. 2019, A&A, 624, A24
Carretta, E., Bragaglia, A., Gratton, R., & Lucatello, S. 2009a, A&A, 505, 139
Carretta, E., Bragaglia, A., Gratton, R. G., et al. 2009b, A&A, 505, 117
Carretta, E., Bragaglia, A., Gratton, R. G., et al. 2010, ApJL, 714, L7
Carrillo, A., Deason, A. J., Fattahi, A., Callingham, T. M., & Grand, R. J. J. 2024, MNRAS, 527, 2165
Casamiquela, L., Castro-Ginard, A., Anders, F., & Soubiran, C. 2021, A&A, 654, A151
Charbonnel, C., & Prantzos, N. 2006, arXiv:astro-ph/0606220
Cheng, Z., Li, Z., Wang, W., Li, X., & Xu, X. 2020, ApJ, 904, 198
Chiba, M., & Beers, T. C. 2000, AJ, 119, 2843
Cordoni, G., Da Costa, G. S., Yong, D., et al. 2021, MNRAS, 503, 2539
Cunha, K., Smith, V. V., Hasselquist, S., et al. 2017, ApJ, 844, 145
Da Costa, G. S., & Coleman, M. G. 2008, AJ, 136, 506
De Silva, G. M., Freeman, K. C., Bland-Hawthorn, J., et al. 2015, MNRAS, 449, 2604
Deason, A. J., Belokurov, V., Koposov, S. E., & Lancaster, L. 2018, ApJL, 862, L1
Denissenkov, P. A., Da Costa, G. S., Norris, J. E., & Weiss, A. 1998, A&A, 333, 926
Dinescu, D. I. 2002, in ASP Conf. Ser. 265, Omega Centauri, A Unique Window into Astrophysics, ed. F. van Leeuwen, J. D. Hughes, & G. Piotto (San Francisco, CA: ASP), 365
Donlon, T., & Newberg, H. J. 2023, ApJ, 944, 169
Donlon, T., Newberg, H. J., Sanderson, R., et al. 2024, MNRAS, 531, 1422
Eilers, A.-C., Hogg, D. W., Rix, H.-W., & Ness, M. K. 2019, ApJ, 871, 120
Eisenstein, D. J., Weinberg, D. H., Agol, E., et al. 2011, AJ, 142, 72
Fattahi, A., Belokurov, V., Deason, A. J., et al. 2019, MNRAS, 484, 4471
Fernández-Trincado, J. G., Vivas, A. K., Mateu, C. E., et al. 2015, A&A, 574, A15
Fernández-Trincado, J. G., Zamora, O., García-Hernández, D. A., et al. 2017, ApJL, 846, L2
Ferraro, F. R., Bellazzini, M., & Pancino, E. 2002, ApJL, 573, L95
Feuillet, D. K., Feltzing, S., Sahlholdt, C. L., & Casagrande, L. 2020, MNRAS, 497, 109
Forbes, D. A. 2020, MNRAS, 493, 847
Forbes, D. A., & Kroupa, P. 2011, PASA, 28, 77
Freeman, K., & Bland-Hawthorn, J. 2002, ARA&A, 40, 487
Gaia Collaboration, Brown, A. G. A., Vallenari, A., et al. 2021, A&A, 649, A1
Gaia Collaboration, Vallenari, A., Brown, A. G. A., et al. 2023, A&A, 674, A1
Garcia-Dias, R., Allende Prieto, C., Sánchez Almeida, J., & Alonso Palicio, P. 2019, A&A, 629, A34
García Pérez, A. E., Allende Prieto, C., Holtzman, J. A., et al. 2016, AJ, 151, 144
Geisler, D., Wallerstein, G., Smith, V. V., & Casetti-Dinescu, D. I. 2007, PASP, 119, 939
Gratton, R., Sneden, C., & Carretta, E. 2004, ARA&A, 42, 385
Gratton, R. G., Johnson, C. I., Lucatello, S., D'Orazi, V., & Pilachowski, C. 2011, A&A, 534, A72
Gratton, R. G., Sneden, C., Carretta, E., & Bragaglia, A. 2000, A&A, 354, 169
Gunn, J. E., Siegmund, W. A., Mannery, E. J., et al. 2006, AJ, 131, 2332
Gustafsson, B., Edvardsson, B., Eriksson, K., et al. 2008, A&A, 486, 951
Häberle, M., Neumayer, N., Seth, A., et al. 2024, Natur, 631, 285
Hasselquist, S., Carlin, J. L., Holtzman, J. A., et al. 2019, ApJ, 872, 58
Hasselquist, S., Hayes, C. R., Lian, J., et al. 2021, ApJ, 923, 172
Hasselquist, S., Shetrone, M., Cunha, K., et al. 2016, ApJ, 833, 81
Hayes, C. R., Majewski, S. R., Hasselquist, S., et al. 2020, ApJ, 889, 63
Hayes, C. R., Majewski, S. R., Shetrone, M., et al. 2018, ApJ, 852, 49
Haywood, M., Di Matteo, P., Lehnert, M. D., et al. 2018, ApJ, 863, 113
Helmi, A., Babusiaux, C., Koppelman, H. H., et al. 2018, Natur, 563, 85
Hogg, D. W., Casey, A. R., Ness, M., et al. 2016, ApJ, 833, 262
Holtzman, J. A., Hasselquist, S., Shetrone, M., et al. 2018, AJ, 156, 125
Holtzman, J. A., Shetrone, M., Johnson, J. A., et al. 2015, AJ, 150, 148
Horta, D., Schiavon, R. P., Mackereth, J. T., et al. 2021, MNRAS, 500, 1385
Horta, D., Schiavon, R. P., Mackereth, J. T., et al. 2023, MNRAS, 520, 5671
Howes, L. M., Asplund, M., Keller, S. C., et al. 2016, MNRAS, 460, 884
Hubeny, I., Allende Prieto, C., Osorio, Y., & Lanz, T. 2021, arXiv:2104.02829

Ibata, R. A., Bellazzini, M., Malhan, K., Martin, N., & Bianchini, P. 2019, NatAs, 3, 667
Ideta, M., & Makino, J. 2004, ApJL, 616, L107
Jean-Baptiste, I., Di Matteo, P., Haywood, M., et al. 2017, A&A, 604, A106
Johnson, C. I., & Pilachowski, C. A. 2010, ApJ, 722, 1373
Jönsson, H., Holtzman, J. A., Allende Prieto, C., et al. 2020, AJ, 160, 120
Koppelman, H. H., Bos, R. O. Y., & Helmi, A. 2020, A&A, 642, L18
Kos, J., Bland-Hawthorn, J., Freeman, K., et al. 2018, MNRAS, 473, 4612
Kuzma, P. B., & Ishigaki, M. N. 2025, MNRAS, 537, 2752
Law, D. R., Majewski, S. R., Skrutskie, M. F., Carpenter, J. M., & Ayub, H. F. 2003, AJ, 126, 1871
Layden, A. C., & Sarajedini, A. 2000, AJ, 119, 1760
Lee, Y. W., Joo, J. M., Sohn, Y. J., et al. 1999, Natur, 402, 55
Leon, S., Meylan, G., & Combes, F. 2000, A&A, 359, 907
Limberg, G., Souza, S. O., Pérez-Villegas, A., et al. 2022, ApJ, 935, 109
Mackereth, J. T., Schiavon, R. P., Pfeffer, J., et al. 2019, MNRAS, 482, 3426
Majewski, S. R., Hasselquist, S., Łokas, E. L., et al. 2013, ApJL, 777, L13
Majewski, S. R., Nidever, D. L., Smith, V. V., et al. 2012, ApJL, 747, L37
Majewski, S. R., Patterson, R. J., Dinescu, D. I., et al. 2000, in Liege Int. Astrophysical Coll. 35, The Galactic Halo: From Globular Cluster to Field Stars, ed. A. Noels et al. (Liege: Inst. d'Astrophysique et de Geophysique), 619
Majewski, S. R., Schiavon, R. P., Frinchaboy, P. M., et al. 2017, AJ, 154, 94
Majewski, S. R., Skrutskie, M. F., Weinberg, M. D., & Ostheimer, J. C. 2003, ApJ, 599, 1082
Marino, A. F., Milone, A. P., Karakas, A. I., et al. 2015, MNRAS, 450, 815
Marino, A. F., Milone, A. P., Piotto, G., et al. 2009, A&A, 505, 1099
Marino, A. F., Milone, A. P., Piotto, G., et al. 2012, ApJ, 746, 14
Martell, S. L., Shetrone, M. D., Lucatello, S., et al. 2016, ApJ, 825, 146
Mason, A. C., Schiavon, R. P., Kamann, S., et al. 2025, MNRAS, submitted (arXiv:2504.06341)
Massari, D., Koppelman, H. H., & Helmi, A. 2019, A&A, 630, L4
Mészáros, S., Masseron, T., Fernández-Trincado, J. G., et al. 2021, MNRAS, 505, 1645
Mészáros, S., Masseron, T., García-Hernández, D. A., et al. 2020, MNRAS, 492, 1641
Meza, A., Navarro, J. F., Abadi, M. G., & Steinmetz, M. 2005, MNRAS, 359, 93
Miki, Y., & Umemura, M. 2017, NewA, 52, 65
Miki, Y., & Umemura, M. 2018, MNRAS, 475, 2269
Mitschang, A. W., De Silva, G., Sharma, S., & Zucker, D. B. 2013, MNRAS, 428, 2321
Mitschang, A. W., De Silva, G., Zucker, D. B., et al. 2014, MNRAS, 438, 2753
Monaco, L., Bellazzini, M., Ferraro, F. R., & Pancino, E. 2005, MNRAS, 356, 1396
Morrison, H. L., Flynn, C., & Freeman, K. C. 1990, AJ, 100, 1191
Myeong, G. C., Evans, N. W., Belokurov, V., Sanders, J. L., & Koposov, S. E. 2018, ApJL, 863, L28
Myeong, G. C., Vasiliev, E., Iorio, G., Evans, N. W., & Belokurov, V. 2019, MNRAS, 488, 1235
Naidu, R. P., Conroy, C., Bonaca, A., et al. 2020, ApJ, 901, 48
Ness, M., Rix, H., Hogg, D. W., et al. 2018, ApJ, 853, 198

Nidever, D. L., Hasselquist, S., Hayes, C. R., et al. 2020, ApJ, 895, 88
Nidever, D. L., Holtzman, J. A., Allende Prieto, C., et al. 2015, AJ, 150, 173
Norris, J. 1986, ApJS, 61, 667
Norris, J. E., & Da Costa, G. S. 1995, ApJ, 447, 680
Norris, M. A., & Kannappan, S. J. 2011, MNRAS, 414, 739
Noyola, E., Gebhardt, K., & Bergmann, M. 2008, ApJ, 676, 1008
Osorio, Y., Allende Prieto, C., Hubeny, I., Mészáros, S., & Shetrone, M. 2020, A&A, 637, A80
Pagnini, G., Di Matteo, P., Haywood, M., et al. 2025, A&A, 693, A155
Pancino, E., Ferraro, F. R., Bellazzini, M., Piotto, G., & Zoccali, M. 2000, ApJL, 534, L83
Pancino, E., Romano, D., Tang, B., et al. 2017, A&A, 601, A112
Pfeffer, J., Lardo, C., Bastian, N., Saracino, S., & Kamann, S. 2021, MNRAS, 500, 2514
Phillips, S. G., Schiavon, R. P., Mackereth, J. T., et al. 2022, MNRAS, 510, 3727
Piotto, G., Villanova, S., Bedin, L. R., et al. 2005, ApJ, 621, 777
Price-Whelan, A. M. 2017, JOSS, 2, 388
Queiroz, A. B. A., Anders, F., Chiappini, C., et al. 2020, A&A, 638, A76
Queiroz, A. B. A., Chiappini, C., Perez-Villegas, A., et al. 2021, A&A, 656, A156
Quillen, A. C., Anguiano, B., De Silva, G., et al. 2015, MNRAS, 450, 2354
Robin, A. C., Reylé, C., Fliri, J., et al. 2014, A&A, 569, A13
Romano, D., Matteucci, F., Tosi, M., et al. 2007, MNRAS, 376, 405
Santana, F. A., Beaton, R. L., Covey, K. R., et al. 2021, AJ, 162, 303
Sarajedini, A., & Layden, A. C. 1995, AJ, 109, 1086
Schiavon, R. P., Phillips, S. G., Myers, N., et al. 2024, MNRAS, 528, 1393
Schiavon, R. P., Zamora, O., Carrera, R., et al. 2017, MNRAS, 465, 501
Schmidhuber, J. 2014, arXiv:1404.7828
Sellwood, J. A., & Preto, M. 2002, in ASP Conf. Ser. 275, Disks of Galaxies: Kinematics, Dynamics and Peturbations, ed. E. Athanassoula, A. Bosma, & R. Mujica (San Francisco, CA: APS), 281
Shetrone, M., Bizyaev, D., Lawler, J., et al. 2015, ApJS, 221, 24
Siegel, M. H., Dotter, A., Majewski, S. R., et al. 2007, ApJL, 667, L57
Simpson, J. D., Martell, S. L., Da Costa, G., et al. 2020, MNRAS, 491, 3374
Smith, V. V., Bizyaev, D., Cunha, K., et al. 2021, AJ, 161, 254
Smith, V. V., Suntzeff, N. B., Cunha, K., et al. 2000, AJ, 119, 1239
Spina, L., Magrini, L., Sacco, G. G., et al. 2022, A&A, 668, A16
Tsuchiya, T., Dinescu, D. I., & Korchagin, V. I. 2003, ApJL, 589, L29
Tsuchiya, T., Korchagin, V. I., & Dinescu, D. I. 2004, MNRAS, 350, 1141
van der Maaten, L., & Hinton, G. E. 2008, Journal of Machine Learning Research, 9, 2579, https://jmlr.org/papers/v9/vandermaaten08a.html
Vasiliev, E. 2019, MNRAS, 484, 2832
Villalobos, Á., & Helmi, A. 2009, MNRAS, 399, 166
Villanova, S., Geisler, D., Gratton, R. G., & Cassisi, S. 2014, ApJ, 791, 107
Webb, J. J., Price-Jones, N., Bovy, J., et al. 2020, MNRAS, 494, 2268
Wilson, J. C., Hearty, F. R., & Skrutskie, M. F. 2019, PASP, 131, 055001
Wylie, S. M., Gerhard, O. E., Ness, M. K., et al. 2021, A&A, 653, A143
Wylie-de Boer, E., Freeman, K., & Williams, M. 2010, AJ, 139, 636
Yong, D., Roederer, I. U., Grundahl, F., et al. 2014, MNRAS, 441, 3396
Youakim, K., Lind, K., & Kushniruk, I. 2023, MNRAS, 524, 2630
Zasowski, G., Cohen, R. E., Chojnowski, S. D., et al. 2017, AJ, 154, 198